

Jie-Mei Wang,^{1,2} Yining Qiu,¹ Zeng-quan Yang,³ Li Li,^{1,4} and Kezhong Zhang^{1,3,5}

Inositol-Requiring Enzyme 1 Facilitates Diabetic Wound Healing Through Modulating MicroRNAs



Diabetes 2017;66:177–192 | DOI: 10.2337/db16-0052

Diabetic skin ulcers represent a challenging clinical problem with mechanisms not fully understood. In this study, we investigated the role and mechanism for the primary unfolded protein response (UPR) transducer inositol-requiring enzyme 1 (IRE1 α) in diabetic wound healing. Bone marrow-derived progenitor cells (BMPCs) were isolated from adult male type 2 diabetic and their littermate control mice. In diabetic BMPCs, IRE1 α protein expression and phosphorylation were repressed. The impaired diabetic BMPC angiogenic function was rescued by adenovirus-mediated expression of IRE1 α but not by the RNase-inactive IRE1 α or the activated X-box binding protein 1 (XBP1), the canonical IRE1 α target. In fact, IRE1 α RNase processes a subset of microRNAs (miRs), including miR-466 and miR-200 families, through which IRE1 α plays an important role in maintaining BMPC function under the diabetic condition. IRE1 α attenuated maturation of miR-466 and miR-200 family members at precursor miR levels through the regulated IRE1 α -dependent decay (RIDD) independent of XBP1. IRE1 α deficiency in diabetes resulted in a burst of functional miRs from miR-466 and miR-200 families, which directly target and repress the mRNA encoding the angiogenic factor angiopoietin 1 (ANGPT1), leading to decreased ANGPT1 expression and disrupted angiogenesis. Importantly, cell therapies using IRE1 α -expressing BMPCs or direct IRE1 α gene transfer significantly accelerated cutaneous wound healing in diabetic mice through facilitating angiogenesis. In conclusion, our studies revealed a novel mechanistic basis for

rescuing angiogenesis and tissue repair in diabetic wound treatments.

Diabetic skin ulcers represent a challenging clinical problem that often results in amputation (1). Neovascularization is one of the rate-limiting steps of wound healing, but it is found aberrant in wound beds in patients with diabetes with unclear mechanisms (2). Bone marrow-derived progenitor cells (BMPCs) are an important endogenous repair reservoir for neovascularization (3). It is believed that therapies of stem/progenitor cells targeting angiogenesis are hopeful solutions for refractory tissue repair. However, the dysfunction of patient-derived progenitor cells has been implicated in diabetes, which represents a major obstacle to the eventual success of autologous cell therapies in the clinic (4,5).

Metabolic stress associated with diabetes, for example, hyperglycemia, hyperlipidemia, and inflammatory cytokines (6,7), imposes cellular stress on the endoplasmic reticulum (ER) and may cause accumulation of unfolded or misfolded proteins in the ER lumen. These conditions can trigger the unfolded protein response (UPR), leading to activation of three major ER transmembrane sensors, including inositol-requiring enzyme 1 (IRE1 α), protein kinase RNA-like ER kinase (PERK), and activating transcription factor 6 (ATF6) (8). Among others, IRE1 α is a primary UPR transducer that, when activated by autophosphorylation, functions as an RNase and executes an unconventional splicing of the mRNA encoding a potent transcription factor X-box binding

¹Center for Molecular Medicine and Genetics, Wayne State University, Detroit, MI

²Department of Pharmaceutical Sciences, Eugene Applebaum College of Pharmacy and Health Sciences, Wayne State University, Detroit, MI

³Karmanos Cancer Institute, Wayne State University, Detroit, MI

⁴Department of Internal Medicine, Wayne State University School of Medicine, Detroit, MI

⁵Department of Immunology and Microbiology, Wayne State University School of Medicine, Detroit, MI

Corresponding authors: Jie-Mei Wang, jiemei.wang@wayne.edu, and Kezhong Zhang, kzhang@med.wayne.edu.

Received 11 January 2016 and accepted 9 September 2016.

This article contains Supplementary Data online at <http://diabetes.diabetesjournals.org/lookup/suppl/doi:10.2337/db16-0052/-/DC1>.

© 2017 by the American Diabetes Association. Readers may use this article as long as the work is properly cited, the use is educational and not for profit, and the work is not altered. More information is available at <http://www.diabetesjournals.org/content/license>.

See accompanying article, p. 23.

protein 1 (XBP1), which activates expression of the genes primarily involved in the UPR signaling. In addition to processing the XBP1 mRNA, IRE1 α can process select mRNAs or microRNAs (miRNAs) and subsequently lead to their degradation, a process known as regulated IRE1 α -dependent decay (RIDD) (9–11). Upon activation of the RIDD pathway, IRE1 α recognizes unique G/C sites within the stem-loop structures of select pre-miRNAs and initiates unconventional cleavage of the substrates. This action counteracts the cleavage and processing by the RNase Dicer, causing the pre-miRNAs to be degraded. Recent research suggested that IRE1 α -mediated cleavage of XBP1 and RIDD of mRNAs or miRNAs are separable activities that are associated with distinct IRE1 α conformational changes and affinities to the substrates (12). A unique role has been speculated for IRE1 α in diabetes-related complications because of the observation that IRE1 α activities are attenuated during persistent ER stress (13,14). However, the exact downstream targets of IRE1 α and the mechanisms of IRE1 α -mediated UPR in diabetes-associated wound healing disorders are poorly characterized.

miRNAs are small noncoding RNAs that act as key post-transcriptional regulators of gene expression by base pairing to the 3' untranslated region (3'-UTR) of their target mRNAs, thereby mediating mRNA translational repression or cleavage (15). miRNAs have been shown to be involved in a wide range of biological processes with highly tissue-specific expression and distinct temporal expression patterns (15). Our previous reports demonstrate that miRNAs are important gene regulators in angiogenesis mediated by BMPCs in type 2 diabetes (16,17). Whereas most of the current research efforts are focused on identifying the downstream targets of miRNAs, the upstream mechanisms through which miRNAs are regulated remain largely unknown. It was not until recently that the importance of miRNAs in ER stress-induced pathogenesis has been recognized (18,19). However, it is unclear whether IRE1 α plays a role in regulating miR expression in type 2 diabetes.

In this study, we reported an important biological function of IRE1 α beyond its canonical role in mediating ER stress response in diabetes. Attenuation of IRE1 α RNase activity resulted in an increase of a subset of miRNAs in diabetes, leading to impaired BMPC angiogenic functions, which cannot be reversed by restoring IRE1 α 's canonical downstream target XBP1. We further uncovered that the IRE1 α -mediated miR repression occurred at the pre-miR level and led to increased functional miRNAs that exerted the translational block on expression of the proangiogenic factor angiopoietin 1 (ANGPT1). The findings from this study not only advance our understanding of the cause of impaired angiogenesis in diabetes but also provide a novel therapeutic strategy for diabetic wound healing by enhancing IRE1 α activity.

RESEARCH DESIGN AND METHODS

Animals

Male type 2 diabetic mice (BKS.Cg-m^{+/+} Lepr^{db}/J, db/db, age 10–12 weeks, plasma glucose 362.23 \pm 41.12 mg/dL)

and their age- and sex-matched nondiabetic healthy littermates (BKS.Cg-m^{-/-} Lep^{db}/- lean, db/+, plasma glucose 160.77 \pm 22.25 mg/dL) were purchased from The Jackson Laboratory (Bar Harbor, ME). IRE1 α ^{flox/flox} (C57BL/6 background) mice were generated as we described previously (20). All animal procedures were performed according to Wayne State University Institutional Animal Care and Use Committee guidelines.

BMPC In Vitro Culture and Adenovirus Infection

In vitro expansion of BMPCs was performed as described in our previous reports (17,21). Bone marrow mononuclear cells from the tibias and femurs of mice were plated on a culture flask coated with rat plasma vitronectin (Sigma-Aldrich) and maintained in endothelial growth media (EGM-2; Lonza) in 37°C, 5% CO₂. For in vitro and in vivo experiments, we used the first passage cells that were cultured for 7 days and ~80% confluent. The following characterization tests have been performed: 1) cell morphology; 2) Ulex-lectin binding and Dil-ac-LDL uptake fluorescent staining; 3) flow cytometry for cell surface markers Sca-1, CD34, Flk-1, Sca-1/Flk-1, VE-cadherin (CD144), CD11b, and CD45; and 4) Western blot analyses for typical endothelial functional protein expressions including VE-cadherin, von Willebrand factor (vWF), and endothelial nitric oxide synthase (eNOS). To generate IRE1 α ^{-/-} BMPCs, BMPCs from IRE1 α ^{flox/flox} mice were infected with adenovirus (Ad)-Cre in order to delete the floxed *Ire1a* exons as we described previously (20). Adenoviral vectors for expression of flag-tagged human IRE1 α (Ad-IRE1 α) were provided by Dr. Yong Liu (Institute for Nutritional Sciences, Shanghai, China). Adenovirus expressing spliced XBP1 was provided by Dr. Umut Ozcan (Harvard University, Cambridge, MA) (22). Adenovirus expressing human ANGPT1 and β -Gal were purchased from Vector Biolabs. For transfection of cells with adenovirus, cells were seeded in six-well plates. After 24 h, cells were transfected with Ad-IRE1 α , Ad-spliced XBP1 (XBP1s), or Ad-GFP at a multiplicity of infection (MOI) of 500 for 48 h as described previously (20).

Transfection of Pre-miR-Expressing Plasmids, Small Interfering RNA, and miR Mimic

Plasmids expressing pre-miR-200 or pre-miR-466 were constructed by inserting human pre-miR-200 and pre-miR-466 sequence into pCMV-miR vector between the SgfI and MluI site (Origene). The empty plasmid served as control. BMPCs were transfected with either 100 ng of the pre-miR-expressing plasmid or the empty plasmid using Lipofectamine 2000 (Life Technologies). Cells were collected simultaneously at 24 h after transfection for further analyses. Small interfering RNA (siRNA) duplexes or miR mimics were transfected into BMPCs with DharmaFECT 1 transfection reagent (Dharmacon) according to the manufacturer's instruction. In each experiment, nonrelated scramble oligo was used as a negative control. After 60 h, the cells were harvested for the experiments.

Quantitative Real-Time PCR Analyses

Total RNA from BMPCs was isolated by miRNeasy Mini Kit (Qiagen). For mRNA expression analysis, quantitative real-time PCR (qRT-PCR) was performed using miR primers synthesized by Exiqon. Amplification and detection of specific miR products were performed with the ABI PRISM 7500 Sequence Detection System, using U6 as an internal control. The C_t value was normalized by subtracting the U6 C_t value, which gave the ΔC_t value. The relative expression levels of each target between groups were then calculated using the following equation: relative gene expression = $2^{-(\Delta C_t_{\text{treatments}} - \Delta C_t_{\text{controls}})}$.

Western Blot Analyses and Detection of IRE1 α Phosphorylation by Phos-tag SDS-PAGE

Total cell lysates were prepared from cultured BMPCs. Denatured proteins were separated by SDS-PAGE on 10% Tris-glycine polyacrylamide gels and transferred to a 0.45-mm polyvinylidene fluoride membrane (GE Healthcare). Levels of β -actin were determined as loading controls. For the detection of phosphorylated IRE1 α , 30 μ g of cell lysates were loaded in 5% Phos-tag SDS-PAGE (Wako Chemicals) according to the manufacturer's instructions (23). Tunicamycin-treated liver lysate was used as positive control. The membrane was incubated with the primary antibodies and horseradish peroxidase-conjugated secondary antibodies. Membrane-bound antibodies were detected by an enhanced chemiluminescence detection reagent (GE Healthcare). The signal intensities were determined by Quantity One 4.4.0 (Bio-Rad, Hercules, CA).

BMPC Functional Assays

In tube formation assay, BMPCs in EBM-2 were plated in a 48-well cell culture plate (5×10^4 cells per well) pre-coated with 150 μ L of growth factor-reduced Matrigel-Matrix (BD Biosciences), as we described previously (17). The migration assay was performed using in vitro scratch assay as described previously (17). Cell proliferation was evaluated using CellTiter 96 Aqueous one solution cell proliferation assay kit (Promega).

miR Array Analysis

Total RNA was extracted from *db/db* BMPCs and *db/+* BMPCs and subjected to mouse genome-wide miR microarray analysis using μ Paraflo Biochip Technology (LC Sciences) based on the latest version of the miRBase database (Sanger miRBase version 21, released 21 July 2014). The array covered all the 1,915 mature sequences of mouse miRs in the miR library. The detailed information of the microarray analysis can be found at the GEO repository (access number GSE72616).

In Vitro IRE1 α -Mediated Pre-miR Cleavage Assay

In vitro cleavage of pre-miR-200 and pre-miR-34 by bioactive, recombinant IRE1 α protein was performed as described previously with modifications (11). In brief, plasmids carrying either human pre-miR-200 sequence or human pre-miR-34 sequence (both from Origene) were used as template for PCR amplification of the linearized DNAs

containing T7 promoter region and pre-miR-200 or pre-miR-34 sequences. The DNA Clean & Concentrator kit (Promega) was used to recover ultrapure DNA from the PCR products. Transcription of large-scale RNAs of pre-miR-200 or pre-miR-34 was performed using the T7 RiboMax Express RNA Production System (Promega). In vitro-transcribed RNA (1 μ g) was incubated with or without 1 μ g bioactive recombinant human IRE1 α protein (SignalChem) in a kinase reaction buffer provided by SignalChem. The cleavage reactions were initiated by adding ATP (2 mmol/L final concentration). Reaction without ATP was used as a control for each sample. After incubation at 37°C for 30 min, the reaction products were resolved on 1.2% denaturing agarose gels and visualized by ethidium bromide staining.

Luciferase 3'-UTR Reporter Assays

The miR-target luciferase reporter assay was performed as previously described (24). Synthetic oligonucleotides of human ANGPT1 mRNA 3'-UTR was cloned into a luciferase reporter vector system (SwitchGear). HEK 293T cells were cotransfected with 100 ng ANGPT1 3'-reporter and 0.1 nmol miR mimics (Exiqon) or 100 ng pre-miR plasmids. After 48 h, luciferase activity was measured, and the relative reporter activity was normalized to that of scramble oligo cotransfection. A reduced firefly luciferase expression indicates the direct binding of miRs to the cloned target sequence.

BMPC Cell Therapy and Gene Therapy for Wound Healing In Vivo

Wounds were created on the dorsal skin of the mouse as previously described (17). Full-thickness skins were removed using a 6-mm punch biopsy without hurting the underlying muscle. For BMPC therapy, immediately after punch, 1×10^6 BMPCs with different gene manipulation in 40 μ L PBS were topically placed onto the wound area. The grouping was as follows: 1) *db/+* wound with PBS, 2) *db/db* wound with PBS, 3) *db/db* wound with *db/+* BMPCs infected with Ad-GFP, 4) *db/db* wound with *db/db* BMPCs infected with Ad-GFP, and 5) *db/db* wound with *db/db* BMPCs transfected with Ad-IRE1 α . For IRE1 α gene transfer, 10^8 particle forming units (pfu) of Ad-IRE1 α or Ad-GFP was preloaded in 40 μ L PBS at 4°C. The adenovirus suspension was injected onto the wound edge in the panniculus carnosus layer immediately after wounding, using a Hamilton syringe and 301/2 gauge needle as described previously (25). The grouping was as following: 1) *db/+* wound with Ad-GFP, 2) *db/db* wound with Ad-GFP, and 3) *db/db* wound with Ad-IRE1 α . Wounds were covered with transparent oxygen-permeable wound dressing (Bioclusive; Johnson & Johnson). The dressings were changed every other day. Wound closure rates were measured by tracing the wound area onto acetate paper. The tracings were digitized, and the areas were calculated with a computerized algorithm and converted to percent wound closure (ImageJ). Wound closure rates were calculated as percentage closed ($y\%$) = [(area on day₀ - open

area on day_x]/area on day₀] \times 100, as we described previously (17). On day 6 after wounding, wounds and the adjacent skin were collected for CD31 immunohistochemistry staining.

Statistics

All values were expressed as mean \pm SEM. The statistical significance of differences between the 2 two groups was determined with Mann-Whitney *U* nonparametric test. When more than two treatment groups were compared, one-way ANOVA followed by least significant difference post hoc testing was used (26). For the in vivo wound closure data, two-way repeated-measures ANOVA followed by Bonferroni post hoc testing was used to compare both differences between treatments and time courses. In all tests, *P* < 0.05 was considered statistically significant.

RESULTS

Reduced IRE1 α Activity in Diabetic BMPCs Is Associated With Impaired BMPC Functions

Bone marrow mononuclear cells were cultured in vitro for 7 days and were characterized as endothelial progenitor cell-enriched population (17,27). The BMPCs we cultured possessed spindle-shaped and cobblestone-like appearances, as well as *Ulex*-lectin binding and *Dil*-ac-LDL uptake double-positive phenotype (Fig. 1A). These are typical characteristics of endothelial lineage. Moreover, these cells displayed increased percentages of Sca-1, CD34, Flk-1, VE-cadherin (CD144), and Sca-1/Flk-1 double staining but decreased percentage of CD11b and unchanged CD45 (Fig. 1B). Western blot analyses indicated that these cells expressed typical functional proteins produced by endothelial cells, such as VE-cadherin, vWF, and eNOS (Fig. 1C). These data confirmed that the cells used in this study were an endothelial progenitor cell-enriched population. To evaluate the involvement of UPR in diabetic BMPCs, we examined the activity of the primary UPR transducer IRE1 α in BMPCs isolated from *db/db* and *db/+* mice. Western blot analyses revealed that the levels of IRE1 α total protein and its phosphorylated form (p-IRE1 α ^{ser-724}) were significantly decreased in *db/db* BMPCs compared with that in the control *db/+* BMPCs (Fig. 1D and E). The reduced levels of the phosphorylated IRE1 α in *db/db* BMPCs were further confirmed by a Phos-tag acrylamide gel that can separate phosphorylated protein from unphosphorylated (Fig. 1F). In comparison, the levels of the other ER stress sensors and mediators, including PERK and ATF6, the chaperone protein BiP (Bip/Grp78), and the ER stress-induced proapoptotic factor CHOP, in *db/db* BMPCs were comparable to those in the *db/+* BMPCs (Fig. 1D and E). We also detected major transcripts in canonical UPR pathways using real-time PCRs (Supplementary Fig. 1). Our data suggested that the canonical UPR pathways in *db/db* type 2 diabetic BMPCs were not activated. The deficiency in IRE1 α RNase activity in diabetes does not alter the UPR signaling mediated through XBP1. To test whether IRE1 α deficiency

leads to BMPC dysfunction, adenoviral vectors expressing flag-tagged full-length human IRE1 α protein (Ad-IRE1 α), its RNase mutant form (Ad-K907A), or its kinase mutant form (Ad-K599A) were used to manipulate IRE1 α RNase activity (20) (Fig. 2A). Meanwhile, the adenovirus expressing the activated form of XBP1 (XBP1s) was used to evaluate the effect of the canonical IRE1 α /XBP1 axis in BMPC function. IRE1 α RNase activity, as indicated by spliced *XBP1* mRNA levels, was significantly increased in BMPCs upon the infection of Ad-IRE1 α , but not by Ad-K907A or Ad-K599A (Fig. 2B). Importantly, IRE1 α overexpression increased the formation of vessel-like tube networks (Fig. 2C and D) and augmented BMPC migration (Fig. 2E) without affecting cell proliferation (Fig. 2F). In contrast, Ad-K907A or Ad-K599A did not induce any of these changes (Fig. 2C–F), suggesting that IRE1 α was critical for BMPC angiogenesis and that the defect in IRE1 α RNase activity contributed to BMPC dysfunction in diabetes. On the other hand, overexpression of the activated form of XBP1 modestly improved cell proliferation (Fig. 2F) with no effect on tube formation or migration (Fig. 2C–E). This evidence suggests that IRE1 α regulates BMPC function independent of activating XBP1. In *db/+* BMPCs, when XBP1 expression was knocked down by siRNA (Fig. 2G), the tube formation of BMPCs was only slightly impaired (Fig. 2H and I).

IRE1 α Deletion Results in the Elevation of a Subset of miRs

To gain mechanistic insights into the role of IRE1 α in the regulation of miRs in diabetic BMPCs, we did a miR microarray in *db/db* and *db/+* BMPCs and identified a subset of miRs that were upregulated in diabetes (*db/db*). The miR microarray analysis revealed that among 44 significantly altered miRs in *db/db* BMPCs, 31 of them were upregulated, including the miR-466 family members (Fig. 3A, framed in red). In addition, qRT-PCR analyses confirmed that the elevation of miR-466 family members and many other miRs that have been implicated in oxidative stress and inflammatory response in diabetes (28), including miR-200 family members (miR-200a/b/c, miR-141, and miR-429), miR-223, miR-155, and miR-34a, in diabetic BMPCs (Fig. 3B). IRE1 α ^{-/-} BMPCs were generated by infecting IRE1 α ^{fllox/fllox} BMPCs with adenovirus expressing CRE recombinase (Fig. 3C). qRT-PCR analyses indicated that deletion of IRE1 α led to a decrease in spliced *XBP1* mRNA but significant increases of many similar miRs that were elevated in diabetic BMPCs, including the miR-466 family, the miR-200 family, miR-155, miR-34a, and miR-223 (Fig. 3D and E). Notably, the miR-466 family has one mature miR member, miR-466 in human, and several mature miR members in mouse, including miR-466s, miR-467s, miR-669s, and miR-297s. The miR-200 family has five mature miR members in both human and mouse, including miR-200a/b/c, miR-141, and miR-429. Examination of the pre-miR sequence of these miRs revealed that they possess G/C splicing sites within the stem loop of the secondary structures, matching the defined cleavage motif sequence

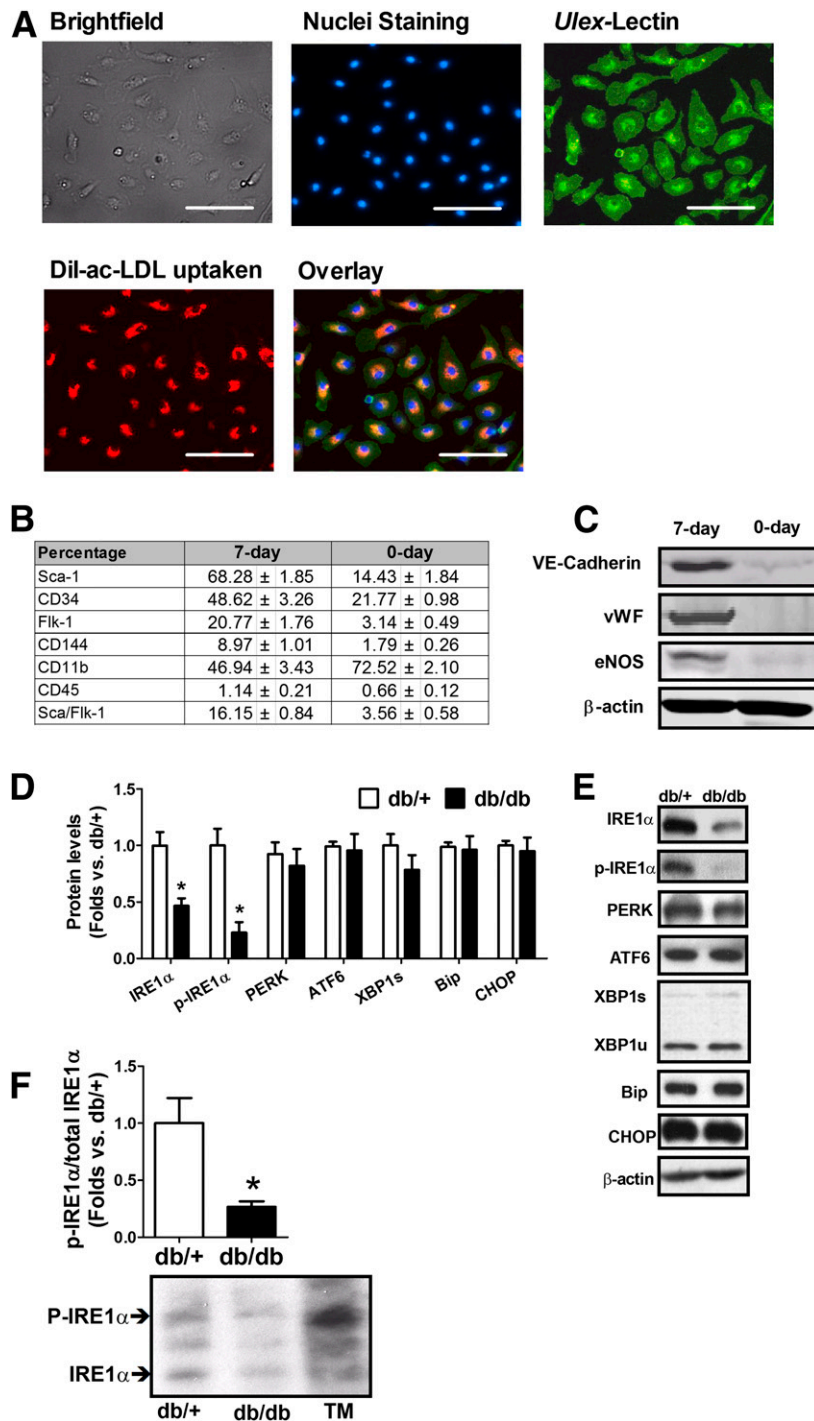


Figure 1—Deficient IRE1 α activity in BMPCs in diabetes. BMPCs from type 2 diabetic *db/db* mice and the healthy control *db/+* mice were cultured in vitro for 7 days. **A**: Fluorescent immunocytochemical staining of *Ulex*-lectin binding and *Dil*-ac-LDL. **B**: Flow cytometry analysis of Sca-1, CD34, Flk-1, VE-cadherin (CD144), and Sca-1/Flk-1 cell surface markers of BMPCs cultured for 7 days. Bar = 100 μ m. **C**: Western blot analysis of protein levels of VE-cadherin, vWF, and eNOS in BMPCs cultured for 7 days. **D**: ER stress response-related protein expressions in *db/db* vs. *db/+* BMPCs. $n = 6$. * $P < 0.05$ vs. *db/+*. **E**: Representative protein bands in *db/+* and *db/db* BMPCs, revealed by Western blot analysis. **F**: Phosphorylated IRE1 α (P-IRE1 α) and unphosphorylated IRE1 α in *db/db* and *db/+* BMPCs separated in Phos-tag gel. $n = 6$. * $P < 0.05$ vs. *db/+*. Representative bands were shown beneath bar graph. Tunicamycin (TM)-treated liver tissue lysate served as a positive control for IRE1 α phosphorylation.

of IRE1 RNase activity (29) (Fig. 3F). In fact, expression of pre-miR-466 or pre-miR-200 in IRE1 α ^{-/-} BMPCs yielded much higher levels of mature miRs than that in the control BMPCs, compared with that in IRE1 α ^{+/+} BMPCs (Fig. 3G

and H). Expression of pre-miR-466 or pre-miR-200 in the IRE1 α ^{-/-} BMPCs infected with Ad-K907A (RNase mutant form of IRE1 α) still yielded higher levels of mature miRs, suggesting that IRE1 α RNase activity is required to

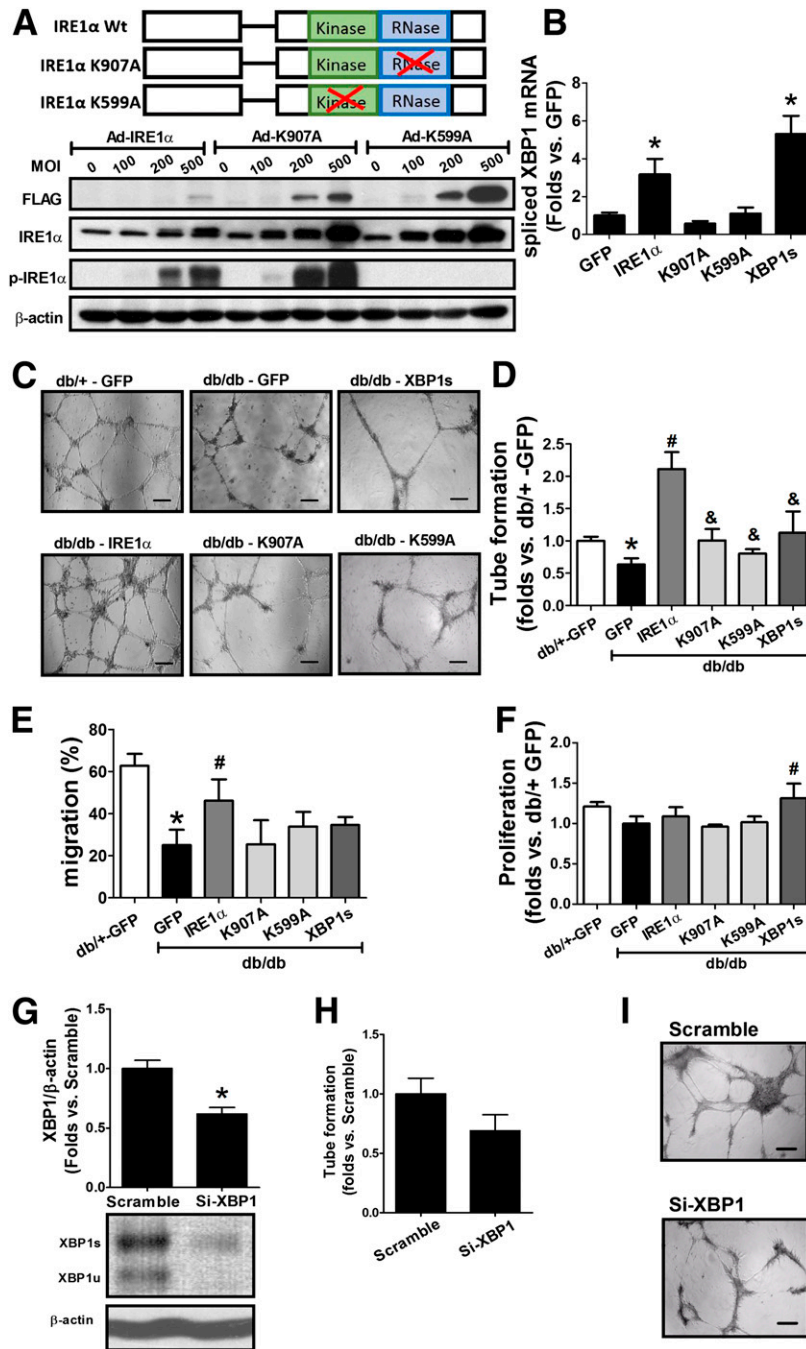


Figure 2—Augmentation of IRE1 α RNase activity boosts BMPC function in diabetes. BMPCs were isolated from individual mice and transfected with flag-tagged Ad-IRE1 α , Ad-K907A, Ad-K599A, or Ad-XBP1s, using adenovirus carrying GFP as controls. Flag-tagged protein and total IRE1 α protein expression were determined by Western blot analysis. The XBP1s mRNA levels were determined by qRT-PCR. **A**: Flag-tagged IRE1 α and total IRE1 α protein expression in *db/db* BMPCs after infection with flag-tagged Ad-IRE1 α , Ad-K907A, or Ad-K599A at 0, 100, 200, 500 MOI for 48 h. **B**: qRT-PCR analysis of XBP1 mRNA splicing in BMPCs infected with Ad-IRE1 α , Ad-K907A, Ad-K599A, or Ad-XBP1s. *n* = 6. **P* < 0.05 vs. Ad-GFP. **C**: Representative pictures showing tube formation of *db/db* BMPCs transfected with Ad-IRE1 α , Ad-K907A, Ad-K599A, Ad-XBP1s, or Ad-GFP at 500 MOI for 48 h, respectively. *db/+* BMPCs transfected with Ad-GFP served as normal controls. Bar = 500 μ m. **D**: Bar graph of tube formation quantification. *n* = 6 per group. **P* < 0.05 vs. *db/+* + Ad-GFP; #*P* < 0.05 vs. *db/db* + Ad-GFP; &*P* < 0.05 vs. *db/db* + Ad-IRE1 α . **E**: Migration of *db/db* BMPCs transfected with Ad-IRE1 α , Ad-K907A, Ad-XBP1s, or Ad-GFP as evaluated by in vitro wound scratch assay. *n* = 5 mice per group. **P* < 0.05 vs. *db/+* + Ad-GFP; #*P* < 0.05 vs. *db/db* + Ad-GFP. **F**: Proliferation of *db/db* BMPCs infected with Ad-IRE1 α , Ad-K907A, Ad-XBP1s, or Ad-GFP as evaluated by CellTiter 96 AQueous Cell Proliferation Assay. *n* = 5 per group. #*P* < 0.05 vs. *db/db* GFP. **G**: Western blot analysis of XBP1 protein in *db/+* BMPCs transfected with XBP1 siRNA (Si-XBP1) or scramble oligo. *n* = 5 mice per group. **P* < 0.05 vs. scramble. **H**: Tube formation in *db/+* BMPCs infected with XBP1 siRNA or scramble oligo. *n* = 5 mice per group. **I**: Representative pictures of tube formation in *db/+* BMPCs transfected with XBP1 siRNA or scramble oligo. Bar = 500 μ m. Wt, wild type.

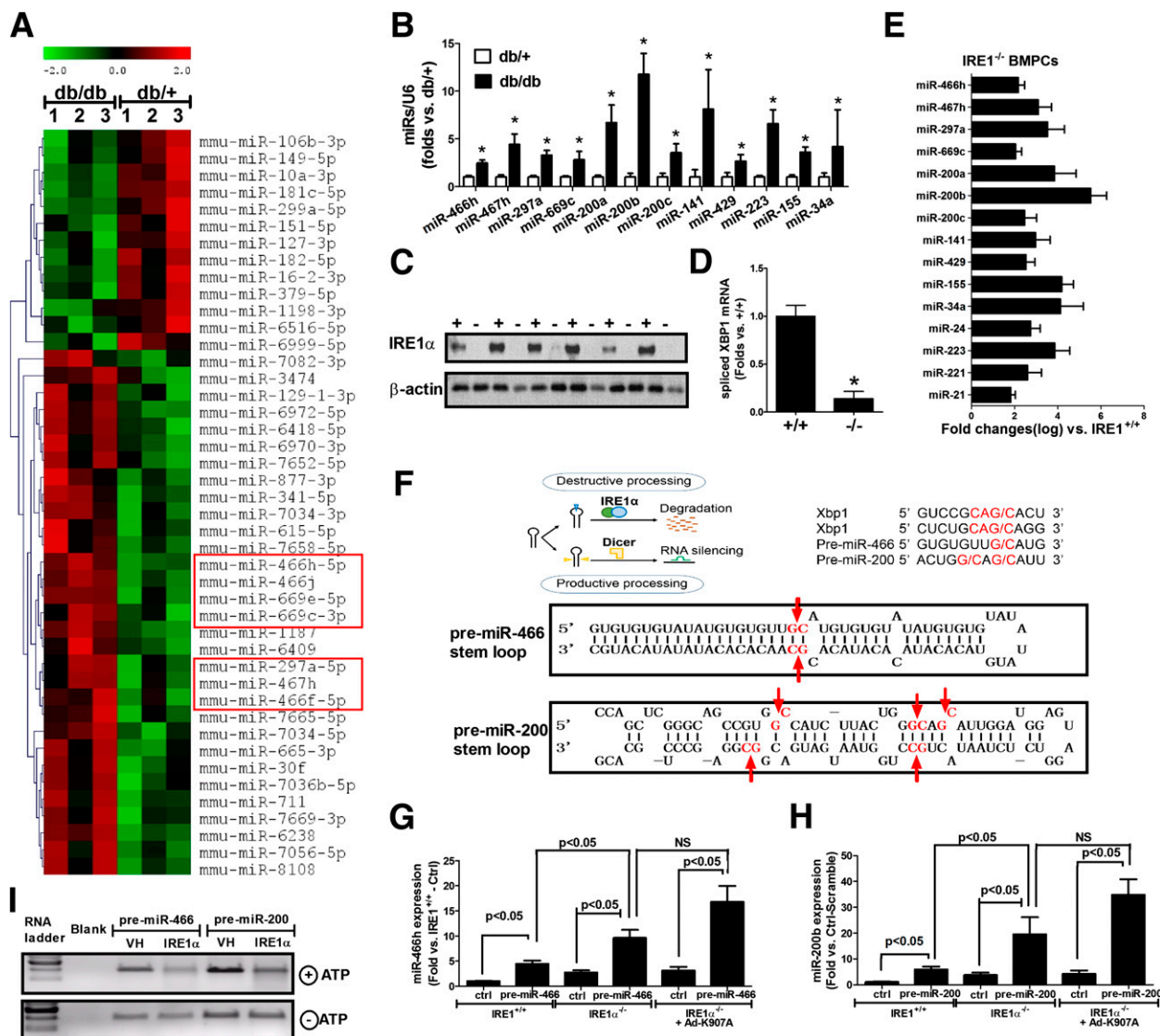


Figure 3—IRE1 α deletion results in the elevation of a subset of miRNos. Total RNA was extracted from *db/db* and *db/+* BMPCs for miR microarray analysis. **A:** Heat map of miR microarray analysis in *db/+* and *db/db* BMPCs. *n* = 3 per group. **B:** qRT-PCR analysis of mature miRNos of miR-466 and miR-200 families as well as miR-223, miR-155, and miR-34a in *db/+* and *db/db* BMPCs. *n* = 7 per group. **P* < 0.05 vs. *db/+*. IRE1 α ^{-/-} BMPCs were generated by infecting IRE1 α ^{fllox/fllox} BMPCs with Ad-CMV-Cre (100 MOI, Ad- β -Gal infection as control IRE1^{+/+} BMPCs). IRE1 α protein expression was determined by Western blot analyses. **C:** IRE1 α protein expression in IRE1^{+/+} and IRE1^{-/-} BMPCs. *n* = 6 per group. **D:** qRT-PCR analysis of XBP1 mRNA splicing in IRE1 α ^{-/-} and IRE1 α ^{+/+} BMPCs. *n* = 6 per group. **P* < 0.05 vs. IRE1 α ^{+/+} BMPCs. **E:** qRT-PCR analysis of mature miRNos in IRE1^{-/-} and IRE1^{+/+} BMPCs. *n* = 6 per group. The elevation of all the miRNos listed in this panel was statistically significant compared to IRE1 α ^{+/+} BMPCs (*P* < 0.05). **F:** Upper left illustration of IRE1 α -mediated miR decay by destroying pre-miR stem-loop structure. Upper right sequence motif and stem-loop structure for the IRE1 α cleavage sites within human XBP1 mRNA, pre-miR-466, and pre-miR-200. Lower pictures show the predicted miR secondary structures for miR-466 and miR-200 with their potential IRE1 α cleavage sites (G/C sites marked with red arrows). **G:** Mature miR expression after pre-miR-466 transfection in either IRE1 α ^{+/+} BMPCs, IRE1 α ^{-/-} BMPCs, or IRE1 α ^{-/-} BMPCs infected with Ad-K907A. Plasmid expressing pre-miR-466 or empty plasmid was transfected into either IRE1 α ^{-/-} or IRE1 α ^{+/+} BMPCs via TurboFECT at the concentration of 100 ng/10⁶ cells. miR-466h was detected using real-time PCRs. *n* = 6 per group. **H:** Mature miR expression after pre-miR-466 transfection in IRE1 α ^{-/-} BMPCs. Plasmid carrying pre-miR-200 or empty plasmid was transfected into either IRE1 α ^{+/+} BMPCs, IRE1 α ^{-/-} BMPCs, or IRE1 α ^{-/-} BMPCs infected with Ad-K907A, via TurboFECT at the concentration of 100 ng/10⁶ cells. Levels of miR-200b were analyzed using qRT-PCR. *n* = 6 per group. **I:** In vitro IRE1 α -mediated pre-miR cleavage assay. In vitro-transcribed pre-miR-200 or pre-miR-466 RNA was incubated with or without recombinant IRE1 α protein in the presence or absence of ATP in the reaction buffer. The cleavage reaction products were resolved on an agarose gel. The reaction without ATP initiation serves as a control for each sample. VH, vehicle buffer that did not contain IRE1 α protein.

suppress mature miR-466 and miR-200. Furthermore, we performed in vitro IRE1 α -mediated RNA cleavage assay by incubating pre-miR-466 or pre-miR-200 with bioactive recombinant human IRE1 α protein. The in vitro cleavage

assay indicated a direct splicing activity of IRE1 α on pre-miR-466 and pre-miR-200, as pre-miR-466 and pre-miR-200 incubated with the recombinant IRE1 α protein were partially degraded (Fig. 3I). Together, this evidence supports

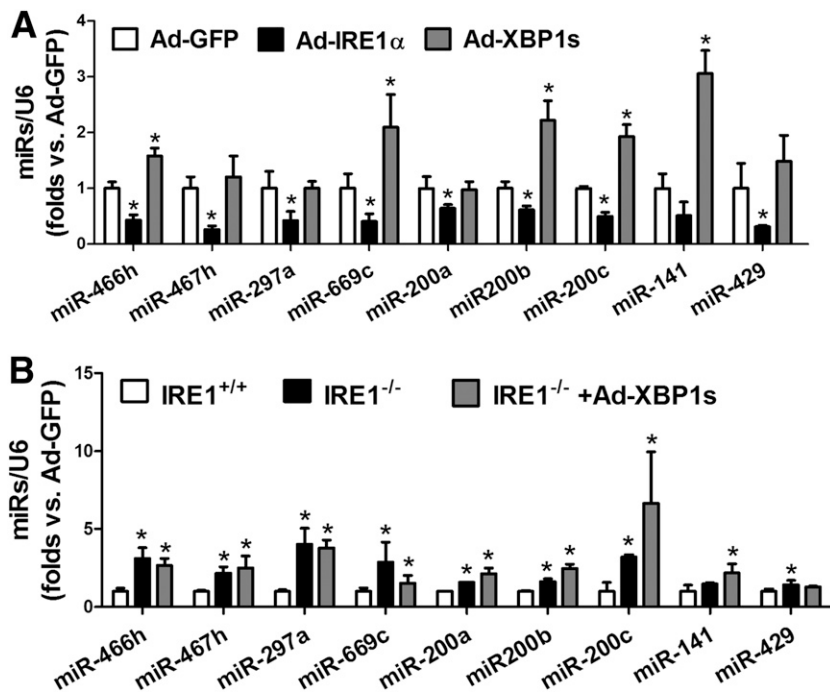


Figure 4—IRE1 α -induced suppression on miR expression is independent of XBP1. BMPCs were isolated from *db/db* mice and transfected with adenovirus carrying IRE1 α , XBP1s, or GFP at 500 MOI for 48 h. qRT-PCR was used to determine miR expressions. **A:** Levels of miR-466 and miR-200 family members in *db/db* BMPCs infected with adenovirus carrying IRE1 α , XBP1s, or GFP. U6 serves as internal control. $n = 5$ mice per group. * $P < 0.05$ vs. Ad-GFP. BMPCs were isolated from individual IRE1 α ^{fl/fl} mice and transfected with Ad-CMV-Cre to delete IRE1 α protein expression; IRE1 α ^{fl/fl} BMPCs transfected with Ad-GFP served as IRE1 α ^{+/+} control. IRE1 α ^{-/-} BMPCs were then transfected with Ad-XBP1s or Ad-GFP at 500 MOI for 48 h. **B:** Levels of miR-466 and miR-200 family members in IRE1 α ^{-/-} BMPCs infected with adenovirus carrying either XBP1s or GFP. $n = 5$ mice per group. * $P < 0.05$ vs. IRE1 α ^{+/+}.

that IRE1 α suppresses production of mature miR-466 and miR-200 family members by targeting their pre-miRs through the RIDD pathway.

IRE1 α -Mediated Suppression of miR Expression Is Independent of XBP1

To verify whether the repression of miR expression by IRE1 α is associated with activation of XBP1, exogenous IRE1 α or the active form of XBP1 was expressed in *db/db* BMPCs using an adenoviral-based overexpression system. Overexpression of IRE1 α significantly repressed the levels of miR-466 and miR-200 family members in *db/db* BMPCs, whereas expression of the activated XBP1 failed to do so (Fig. 4A). Furthermore, we overexpressed the active form of XBP1 in IRE1 α ^{-/-} BMPCs to test whether XBP1 can reverse the expressions of miR-466 and miR-200 family miRs induced by IRE1 α deletion. As shown in Fig. 4B, overexpression of the activated XBP1 did not lower the high expression levels of miR-466 or miR-200 in IRE1 α ^{-/-} BMPCs, suggesting that IRE1 α -mediated miR repression is independent of the IRE1 α -mediated canonical signaling pathway through activating XBP1.

IRE1 α Promotes BMPC Tube Formation by Repressing miR-466 and miR-200

To determine the functional involvement of IRE1 α -mediated suppression of miR-466 and miR-200, pre-miR-466

or pre-miR-200 was transferred into IRE1 α -expressing *db/db* BMPCs to test whether overexpression of one of these two miR families can compromise IRE1 α -induced augmentation of diabetic BMPC function. As shown in Fig. 5A and B, expression of IRE1 α stimulated angiogenesis, as indicated by vessel-like tube formation in *db/db* BMPCs. However, this improvement in angiogenesis was suppressed by overexpression of pre-miR-466, pre-miR-200, or coexpression of pre-miR-466 and pre-miR-200 (Fig. 5A and B), indicating that the role of IRE1 α in preserving angiogenesis and BMPC function is at least partially through repression of miR-466 and miR-200.

Expression of IRE1 α Can Rescue the Defect of ANGPT1, a Direct Target of Both miR-466 and miR-200 Family miRs, in Diabetic BMPCs

Next, we determined the genes targeted by miR-466 and miR-200 under the regulation of IRE1 α in BMPCs. A computer algorithm in PicTar and microRNA.org database indicates that miR members from the miR-466 and miR-200 families, including miR-466, miR-200b, miR-200c, and miR-429, all target the mRNA encoding an important proangiogenic factor, *ANGPT1* (Fig. 6A). *ANGPT1* is a secreted glycoprotein that activates endothelial cell-specific tyrosine-protein kinase (TEK/TIE2) receptor. *ANGPT1* is known to be a key regulator that promotes normal angiogenesis during embryogenesis (30) and restores microvascular

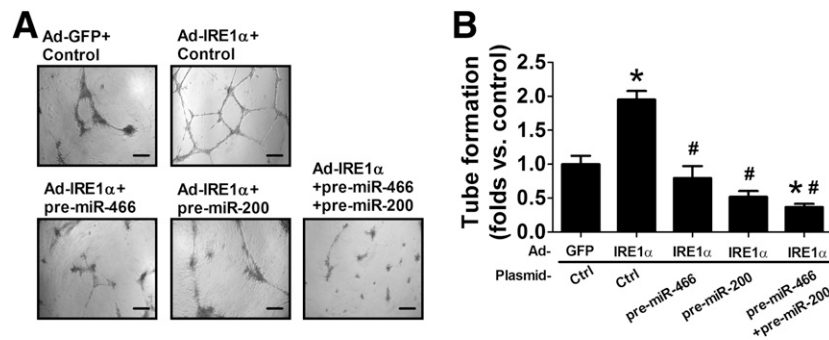


Figure 5—Expression of pre-miR-466 and pre-miR-200 abolish the augmentation of BMPC tube formation induced by IRE1 α overexpression. BMPCs were isolated from type 2 diabetic *db/db* mice and transfected with Ad-GFP or Ad-IRE1 α at 500 MOI for 48 h. Pre-miR-466 or pre-miR-200 or both pre-miR-466 and pre-miR-200 were transfected into IRE1 α -expressing *db/db* BMPCs. BMPC function was evaluated by tube formation on Matrigel. **A**: Representative pictures showing tube formation in IRE1 α -expressing *db/db* BMPCs transfected with empty plasmid (control), pre-miR-466, pre-miR-200, or both pre-miR-466 and pre-miR-200. Bar = 500 μ m. **B**: Bar graph of tube formation quantification. $n = 6$. * $P < 0.05$ vs. *db/db* BMPCs infected with Ad-GFP + control; # $P < 0.05$ vs. *db/db* BMPCs infected with Ad-IRE1 α + control.

function in diabetes (31–33). To verify whether these miRs directly bind to the 3'-UTR of *ANGPT1* mRNA, the complete 3'-UTR sequence of human *ANGPT1* mRNA was introduced into a luciferase reporter system followed by transfection of either pre-miRs or individual mature miRs. The reporter analysis confirmed that *ANGPT1* was the genuine target of miR-466 and miR-200 family miRs, including miR-466, miR-200b/c, and miR-429 (Fig. 6B). Interestingly, whereas each mature miR can modestly suppress the *ANGPT1* mRNA, coexpression of pre-miR-466 and pre-miR-200 exerted much greater repression, implicating the synergetic effects of miRs of the same pre-miR family on the translational control of *ANGPT1* expression. To determine whether IRE1 α regulates *ANGPT1* through the miR pathway, we examined expression of *ANGPT1* mRNA and protein in IRE1 α -expressing *db/db* BMPCs upon transfection with the plasmid vectors expressing pre-miR-266 and pre-miR-200. The qRT-PCR results indicated that upregulation of the *ANGPT1* mRNA, induced by overexpression of IRE1 α , was reversed by expression of pre-miR-466 and/or pre-miR-200 (Fig. 6C). Consistently, Western blot analysis indicated that both pre-miR-466 and pre-miR-200 inhibited expression of *ANGPT1* protein induced by IRE1 α (Fig. 6D). These observations confirm that *ANGPT1* expression is indeed regulated by IRE1 α via suppressing miRs. In fact, *db/db* BMPCs only produced ~50% of *ANGPT1*, compared with *db/+* BMPCs (Fig. 6E). When *ANGPT1* protein was downregulated by ~60% by *ANGPT1* siRNA in *db/+* BMPCs, tube formation by BMPCs was severely impaired (Fig. 6F–H). Conversely, when *ANGPT1* was overexpressed in *db/db* BMPCs (Fig. 6I), the tube formation was restored (Fig. 6J–K). Furthermore, overexpression of IRE1 α significantly augmented *ANGPT1* protein expression in *db/db* BMPCs by ~2.5-fold (Fig. 6L). This evidence supports the essentiality of *ANGPT1* in maintaining BMPC functions in diabetes and indicates

that the *ANGPT1* defect in diabetic BMPCs is largely attributed to the impaired IRE1 α -miR regulatory axis.

Cell Therapy Using Diabetic BMPCs With IRE1 α Overexpression Improves Diabetic Wound Healing In Vivo

Progenitor cells are considered hopeful candidates for cell therapies in regenerative medicine (34,35). Therefore, the efficacy of genetically engineered BMPC therapy was tested in an excisional wound model as we previously established (17). Since our in vitro data showed that overexpression of IRE1 α facilitates angiogenesis and upregulation of *ANGPT1* in diabetic BMPCs, augmenting BMPC-mediated angiogenesis via correcting the IRE1 α deficiency may improve wound healing in diabetic animals. To test this possibility, we infected *db/db* BMPCs with adenovirus expressing IRE1 α for 48 h prior to cell therapies on diabetic wounds. Equal numbers of *db/+* BMPCs or *db/db* BMPCs (10^6) infected with Ad-GFP served as normal and diabetic control cell therapies. Expression of total and phosphorylated IRE1 α as well as *ANGPT1* proteins in the infected BMPCs was confirmed by Western blot analysis (Fig. 7A). As shown in Fig. 7B and C, from day 4 and throughout the healing course, diabetic wounds treated with IRE1 α -expressing *db/db* BMPCs showed significantly faster closure than those treated with GFP-expressing *db/db* BMPCs, with concomitant augmentation of capillary formation as shown by the functional endothelial cell surface marker CD31 staining (day 8 samples) (Fig. 7D, arrows indicate capillary-like structure). Notably, wounds that received IRE1 α -expressing *db/db* BMPCs were healed with a slightly keratinized epithelial layer, whereas wounds that received GFP-expressing *db/db* BMPCs still had large open wound areas (Fig. 7C). The healing curve of IRE1 α -expressing *db/db* BMPC therapy was similar to that of the *db/+* BMPC therapy. This suggests that *IRE1\alpha* gene transfer significantly enhances the therapeutic potential of diabetic BMPCs, achieving efficacy comparable to healthy BMPCs.

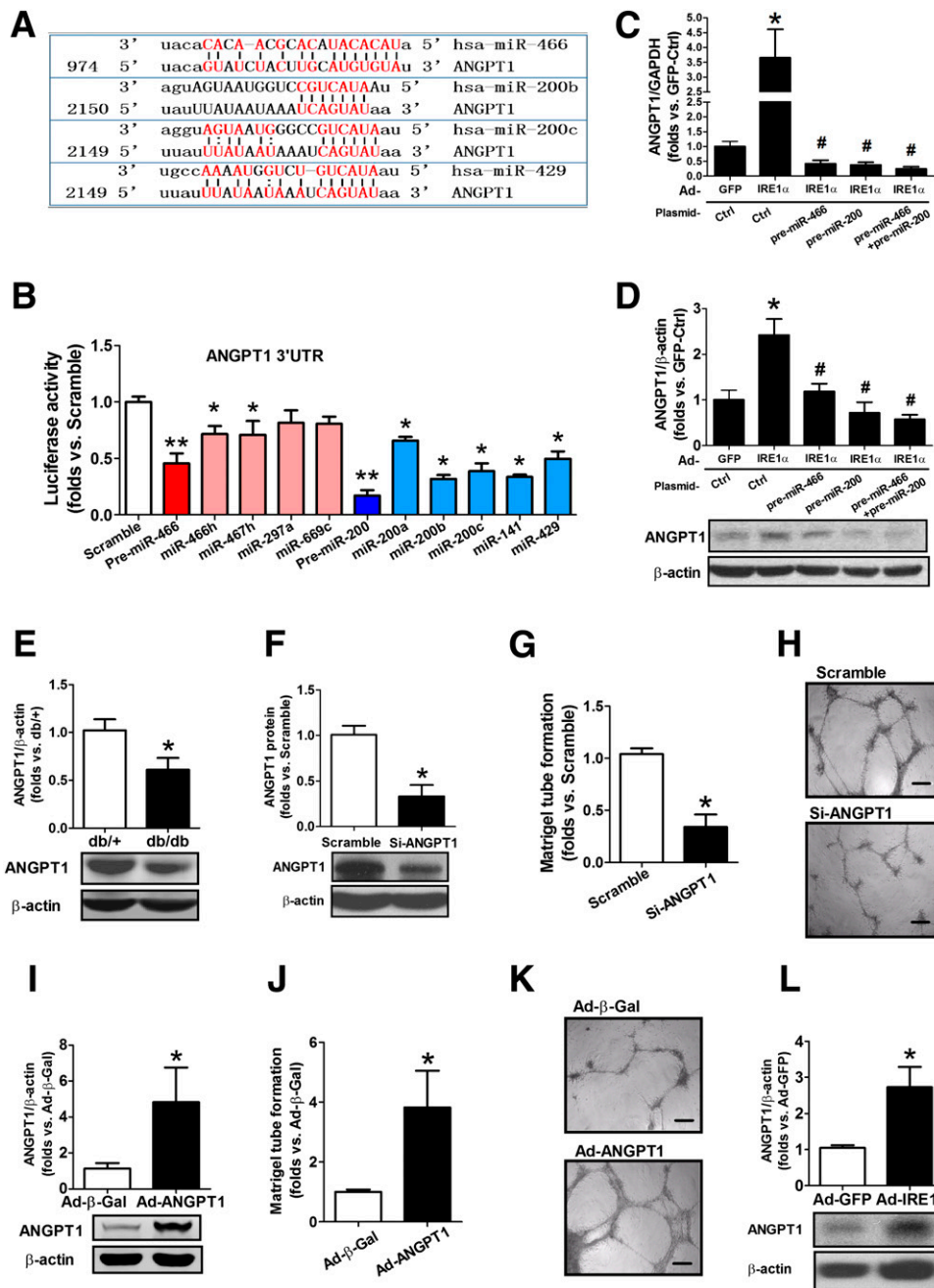


Figure 6—IRE1 α overexpression can rescue the defect of ANGPT1, the direct target of miR-200 and miR-466 members, and impaired angiogenesis in diabetes. Luciferase vector carrying human *ANGPT1* mRNA 3'-UTR sequence was cotransfected with pre-miR-466 or its mature miRs, pre-miR-200 or its mature miRs, or scramble oligo as controls. After 24 h, the cells were collected for detection of luciferase activity. A reduction in luciferase activity indicates direct binding. A: The putative binding sequences of miR-466 and miR-200 in the 3'-UTR of the *ANGPT1* mRNA. The red text indicates the putative binding base pairs between the miRNA and the 3'-UTR of the mRNA based on a computer algorithm. B: Luciferase activities in T293 cells cotransfected with the plasmid vectors expressing the *ANGPT* mRNA 3'-UTR reporter; pre-miR-466; pre-miR-200; individual miRs including miR-466h, miR-200a/b/c/, miR-141, and miR-429; or scramble oligo. $n = 6$. * $P < 0.05$ vs. scramble transfection; ** $P < 0.01$ vs. scramble transfection. C: qRT-PCR analysis of *ANGPT1* mRNA expression in IRE1 α -overexpressing BMPCs transfected with the plasmid vector expressing pre-miR-466 or pre-miR-200 transfection. $n = 6$ mice per group. * $P < 0.05$ vs. GFP-Ctrl; # $P < 0.05$ vs. Ad-IRE1 α -Ctrl. D: Western blot analysis of *ANGPT1* protein in IRE1 α -overexpressing BMPCs transfected with the plasmid vectors expressing pre-miR-466 and pre-miR-200. $n = 6$ mice per group. * $P < 0.05$ vs. GFP-Ctrl; # $P < 0.05$ vs. Ad-IRE1 α -Ctrl. BMPCs were isolated from individual *db/db* or *db/+* mice. *ANGPT1* mRNA levels were determined by qRT-PCR. *ANGPT1* protein expressions were determined by Western blot analysis. The *db/db* BMPCs were transfected with Ad-GFP or Ad-IRE1 α at 500 MOI for 48 h. Pre-miR-466 and pre-miR-200 were transfected into IRE1 α -expressing *db/db* BMPCs. *ANGPT1* mRNA and protein levels were determined by qRT-PCRs and Western blot analyses, respectively. E: *ANGPT1* mRNA expression in *db/db* vs. *db/+* BMPCs. $n = 5$ mice per group. * $P < 0.05$ vs. *db/+*. F: *ANGPT1* protein expression in *db/+* BMPCs transfected with *ANGPT1* siRNA (si) or scramble oligo. $n = 5$ mice per group. * $P < 0.05$ vs. scramble oligo. G: Tube formation in *db/+* BMPCs infected with *ANGPT1* siRNA or scramble oligo. $n = 5$ mice per group. * $P < 0.05$ vs. *db/+* BMPC scramble. H: Representative pictures of tube formation in *db/+* BMPCs transfected

Direct Gene Transfer of IRE1 α Partially Recovers Diabetic Wound Healing In Vivo

Furthermore, we sought to test whether direct *IRE1 α* gene transfer to the wound bed can achieve the same success of *IRE1 α* gene-engineered cell therapies. Immediately after the wounds were created on *db/db* mice, Ad-IRE1 α or Ad-GFP was injected into the wound edge in the panniculus carnosus layer. Our results indicated that Ad-IRE1 α -treated *db/db* wounds displayed accelerated wound closure from day 2, compared with Ad-GFP-treated *db/db* wounds (Fig. 7F and G). The wound capillary formation was also improved by the *IRE1 α* gene transfer (Fig. 7H). By the end of the experiment, Ad-IRE1 α -treated *db/db* wounds were healed by ~70%, whereas Ad-GFP-treated *db/db* wounds were only healed by ~50%, suggesting that *IRE1 α* gene transfer is beneficial to diabetic wound healing. However, the effectiveness of *IRE1 α* gene transfer is modest, since the Ad-IRE1 α -treated *db/db* wounds were healed slower than the Ad-GFP-treated *db/+* wounds (~100% closure on day 16). Apparently, the *IRE1 α* gene transfer in BMPC cell therapy showed much higher efficacy than the *IRE1* gene transfer in local tissue (Fig. 7B and C). These results support the notion that IRE1 α -induced acceleration of the wound healing process is through boosting angiogenic cell activities in diabetic bed sores where the direct *IRE1 α* gene transfer failed to fully exert the effect due to dysfunctional tissues/cells.

DISCUSSION

In this study, we have discovered that IRE1 α promotes the angiogenic potential of diabetic BMPCs through modulating miR biogenesis, which is distinct from its role in mediating canonical UPR. Deficient IRE1 α RNase activity is an important cause of the elevation of a subset of miRs in diabetes, including the miR-466 and miR-200 families, which contributes to the functional impairment of BMPCs. The suppression of miR expression by IRE1 α occurs at the pre-miR level through the RIDD pathway and is not associated with XBP1 activation. The proangiogenic factor ANGPT1 is significantly attenuated in diabetic BMPCs, but the ANGPT1 defect can be rescued by IRE1 α overexpression through repressing miR-466 and miR-200 family miRs. Diabetic BMPC therapies with IRE1 α gene transfer resulted in improved wound capillary formation and fully recovered wound closure in diabetic mice in vivo. In aggregates, our study has demonstrated that deficient IRE1 α RNase activity in diabetes bursts select miR expression, which leads to the suppression of ANGPT1 expression and subsequent disruption of angiogenesis, contributing to an impaired wound healing process (Fig. 8).

It has been suggested that ER stress represents an important aspect of metabolic insults in diabetes (36). Chronic hyperglycemia and hyperlipidemia, two major causative factors of type 2 diabetes, disrupts ER homeostasis and produces excessive unfolded/misfolded proteins in the ER lumen (37). However, differential activation of ER stress sensors may rely on specific stimuli and timing of the ER stress, exerting differential UPR programs. In the context of diabetes-related skin ulcers, the roles of UPR and angiogenesis have been addressed as separate events (38,39), yet little is known about the functional interplay between these two events. In our study, BMPCs from type 2 diabetic *db/db* mice display deficiencies in IRE1 α protein expression, with no change in other ER sensors or canonical UPR signaling pathways, suggesting that the unique change of IRE1 α may be related to the impaired function of BMPCs under the diabetic condition. Current reports suggest that metabolic tissues or cell types, such as liver (hepatocytes), adipose tissue (adipocytes), and pancreas (β -cells), are responding to metabolic stress through canonical UPR pathways (37,40,41). To date, little is known regarding how angiogenic cells, for example, BMPCs, are responding to metabolic stress in diabetes. Our studies demonstrated that metabolic stress regulates ER function in BMPCs through noncanonical UPR pathways, as the IRE α -XBP1 pathway was repressed while other ER stress sensors or downstream pathways remained unchanged (Fig. 1E). Our supplemental data confirmed that the canonical UPR pathways in *db/db* type 2 diabetic BMPCs were not activated (Supplementary Fig. 1). The mechanism by which the IRE1 α -XBP1 pathway is repressed under the diabetic condition is an interesting question. Many pathological changes in both type 1 and type 2 diabetes, such as hyperglycemia, elevated levels of advanced glycation end products (AGEs), oxidative stress, and chronic inflammation, are associated with ER stress response and expression of the ER stress sensor IRE1 α . A recent study showed that obesity-associated chronic inflammation, an inflammatory stress condition found in both type 1 and type 2 diabetes animal models, can repress IRE1 α activity by S-nitrosylation of IRE1 α (42). This may partially explain why type 1 and type 2 diabetes lead to the similar change in IRE1 α expression and activity. In addition to splicing the XBP1 mRNA, IRE1 α can process select mRNAs or pre-miRs, leading to their degradation through the RIDD pathway (9–11). Recent studies suggested that IRE1 α undergoes dynamic conformational changes and switches its functions depending on the duration and types of ER stress (12,13). Under acute ER stress, IRE1 α forms oligomeric clusters to process *XBP1* mRNA splicing during the acute phase. However, under physiological ER stress, IRE1 α 's functional specificity as an RNase shifts to cleaving

with ANGPT1 siRNA or scramble oligo. Bar = 500 μ m. I: ANGPT1 protein expression in *db/db* BMPCs transfected with either Ad- β -Gal or Ad-ANGPT1 at 100 MOI for 48 h. $n = 5$ mice per group. * $P < 0.05$ vs. Ad- β -Gal. J: Tube formation in *db/db* BMPCs transfected with either Ad- β -Gal or Ad-ANGPT1. $n = 5$ per group. * $P < 0.05$ vs. Ad- β -Gal. K: Representative pictures of tube formation in *db/db* BMPCs transfected with either Ad- β -Gal or Ad-ANGPT1. Bar = 500 μ m. L: ANGPT1 protein expression in *db/db* BMPCs infected with either Ad-GFP or Ad-IRE1 α at 500 MOI for 48 h. $n = 5$ per group. * $P < 0.05$ vs. Ad-GFP.

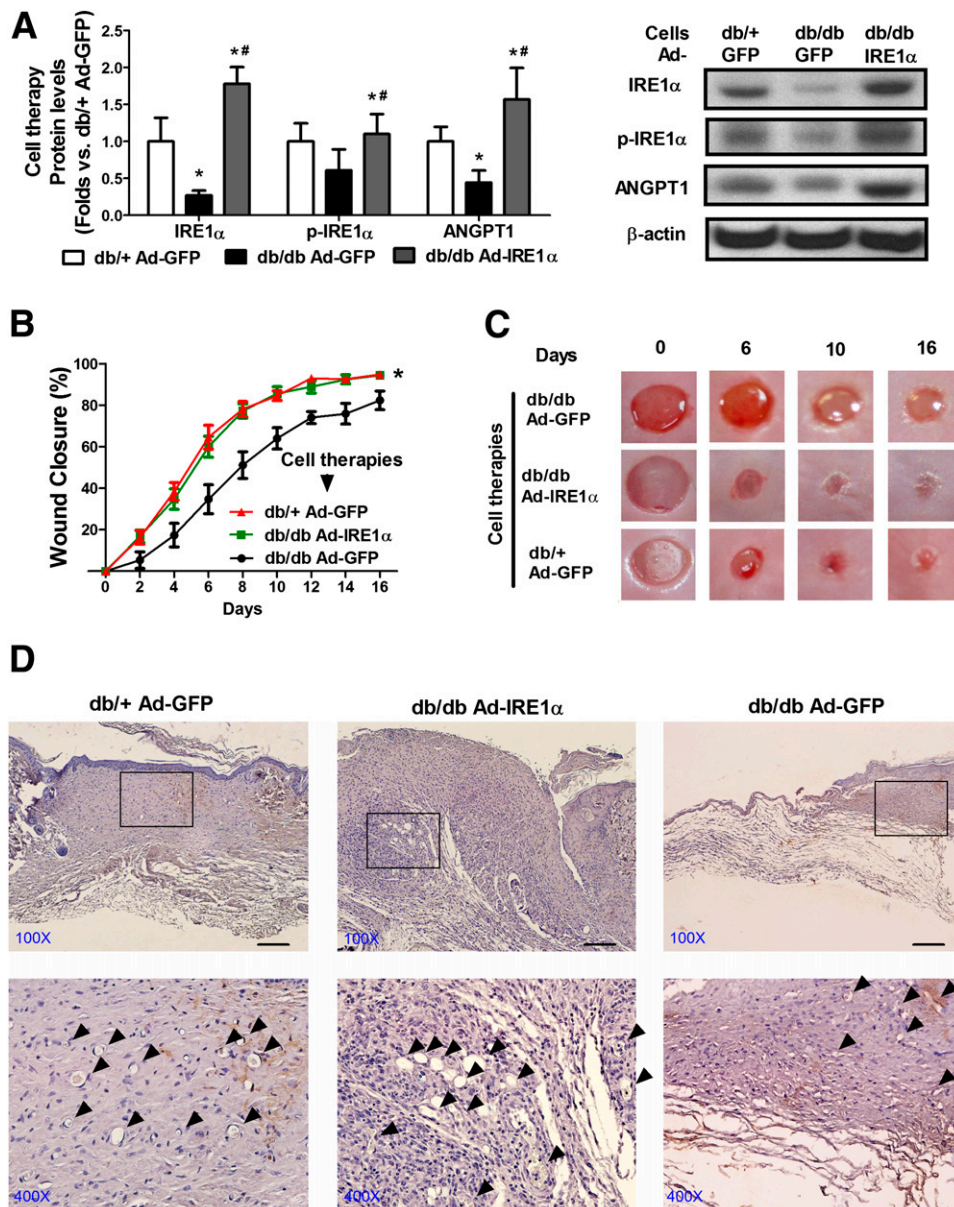


Figure 7—Diabetic cell therapy with IRE1 α overexpression or local gene transfer of IRE1 α improves diabetic wound healing in vivo. Full thickness excisional wound (6 mm) was created on the back of each mouse. For cell therapies, *db/db* BMPCs were infected with Ad-IRE1 α or Ad-GFP at 500 MOI for 48 h. Immediately after wounding, 1×10^6 Ad-IRE1 α - or Ad-GFP-infected BMPCs were transplanted onto *db/db* wounds. For local gene transfer, *db/db* wounds were injected with 1×10^8 particle forming units Ad-IRE1 α or Ad-GFP in 40 μ L PBS solution. Wounds were covered with oxygen-permeable wound dressing (3M). Wound edge was traced and digitalized for percentage calculation. **A**: Western blot analysis of protein expressions of IRE1 α , phosphorylated (p) form of IRE1 α , and ANGPT1 in BMPCs that were used for cell therapies. Representative protein bands were shown on the right side. $n = 5$ per group. * $P < 0.05$ vs. *db/+* + Ad-GFP; # $P < 0.05$ vs. *db/db* + Ad-IRE1 α . **B**: Wound closure curves in *db/db* mice that received BMPC therapies. $n = 5$ mice per group. * $P < 0.05$ vs. *db/db* BMPC + Ad-GFP. **C**: Representative pictures of diabetic wounds after the cell therapy. **D**: Capillary formation as evaluated by CD31 staining (brown) in wounds that received cell therapies. The arrowheads indicated a capillary-like structure at wound edge. Bar = 100 μ m. **E**: Western blot analysis of protein expressions of IRE1 α , phosphorylated form of IRE1 α , and ANGPT1 in wound tissues transfected with either Ad-GFP or Ad-IRE1 α . Representative protein bands were shown on the right side. $n = 5$ per group. * $P < 0.05$ vs. *db/+* + Ad-GFP; # $P < 0.05$ vs. *db/db* + Ad-IRE1 α . **F**: Wound curves of local gene transfer. $n = 5$ mice per group. * $P < 0.05$ vs. *db/db* + Ad-GFP; # $P < 0.05$ vs. *db/+* + Ad-GFP. **G**: Representative pictures of diabetic wounds after the gene therapies. **H**: Capillary formation as evaluated by CD31 staining (brown) in wounds that received gene therapies. The arrowheads indicate a capillary-like structure at wound edge. Bar = 100 μ m.

primarily ER-targeted mRNAs or miRs via the RIDD pathway (9,11,43,44). Additionally, a recent study suggested the existence of mechanisms regulating XBP1 mRNA splicing through modulating recruitment of XBP1 mRNA to ER

membranes (45). Therefore, there might be circumstances in which XBP1 mRNA splicing is not solely dependent on IRE1 α RNase activity. However, when IRE1 α is exogenously overexpressed in mammal cells, for example,

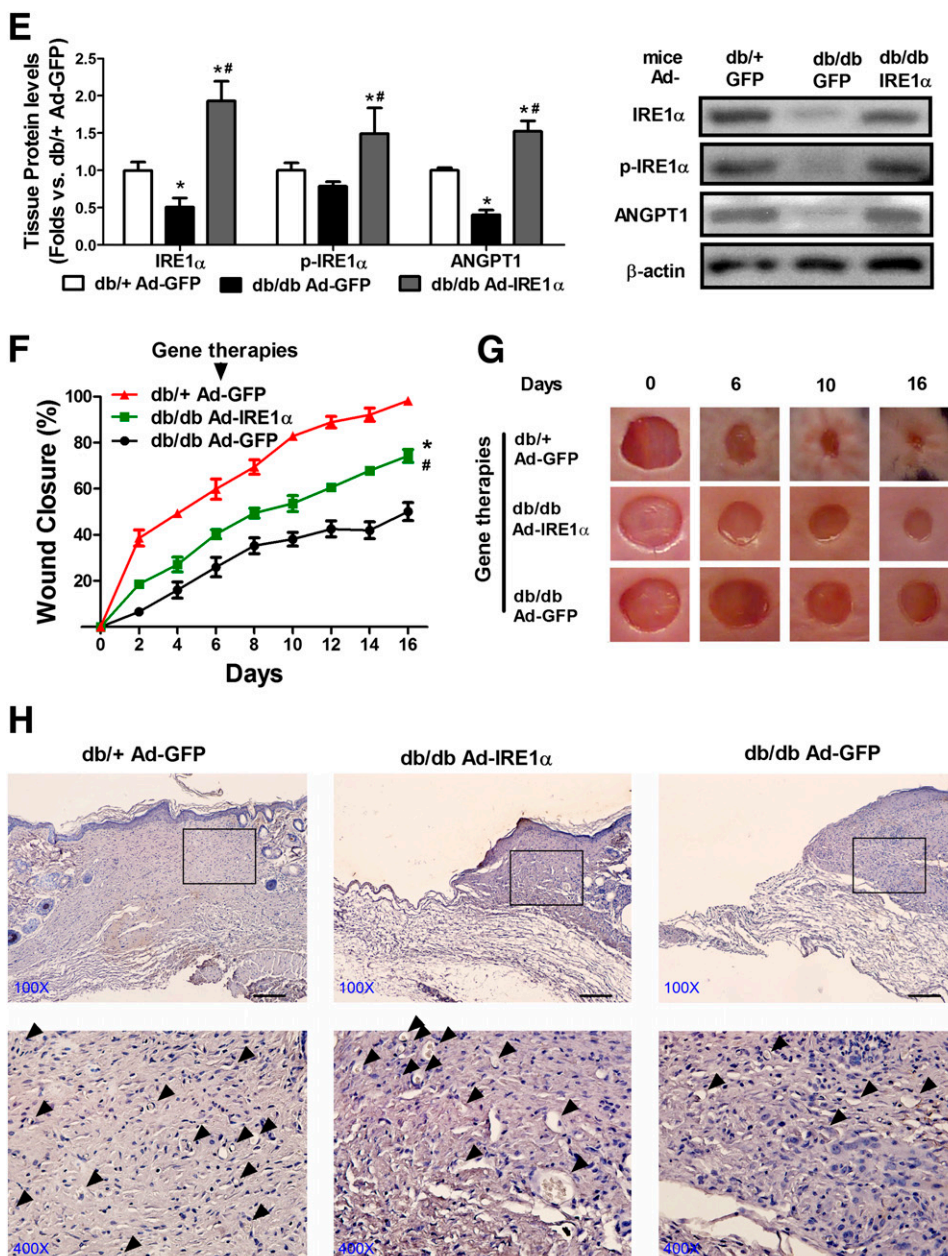


Figure 7—Continued.

adenovirus-mediated gene transfer, what we have observed is that overexpressed IRE1 α functions to splice both *XBP1* mRNA and precursor miRs. Bhatta et al. (46) reported that ER stress markers were elevated in bone marrow endothelial outgrowth cells in *db/db* mice at the age of 15 months, which were considered as aged mice (the life span of *db/db* mice is ~18–20 months). Aging is a significant factor associated with ER stress and the UPR. Along with advanced aging, there is a shift in the balance between the protective adaptive response of the UPR and proapoptotic signaling where the protective arm is significantly reduced and the apoptotic arm is more robust (47). The discrepancy between observation of Bhatta

et al. and ours reflects the dynamic changes in the balance of protective versus detrimental ER stress response in aging or the progression of diabetes.

Another important finding in this study is that the regulation of IRE1 α on BMPC function or miR biogenesis in diabetes is independent of its canonical UPR pathway through activating XBP1. XBP1 is a well-known RNA substrate of IRE1 α under ER stress (48). However, in diabetic BMPCs, in which IRE1 α RNase activity is impaired, *XBP1* mRNA splicing is not altered (Fig. 1D and E). Furthermore, the impaired angiogenesis in diabetic BMPCs can be rescued by overexpression of IRE1 α , but not the activated XBP1 (Fig. 2C and D), thus confirming that XBP1

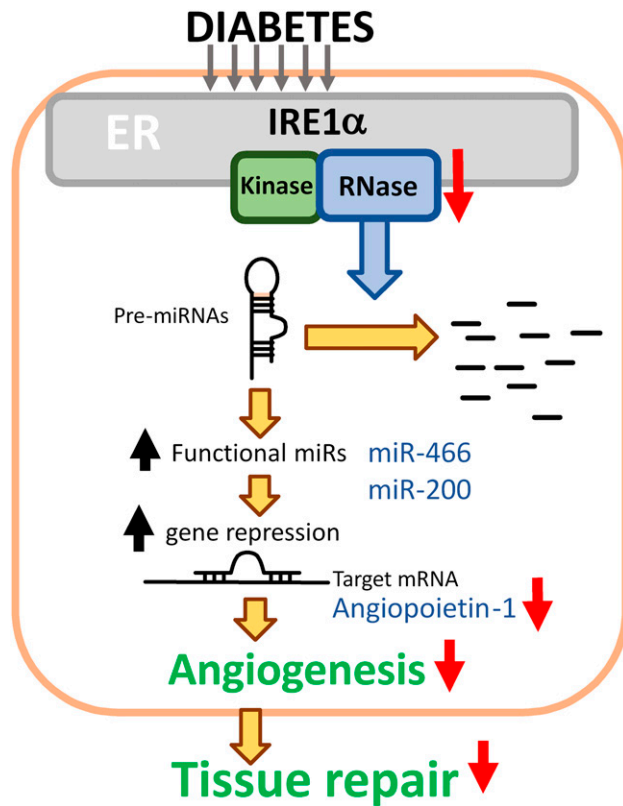


Figure 8—Schema of hypothesis. Under the diabetic condition, IRE1 α RNase activity degrades miR precursors, including pre-miR-466 and pre-miR-200. These two miR families repress *ANGPT1* mRNA translation, leading to downregulation of ANGPT1. Activity of IRE1 α is suppressed in diabetic BMPCs. As a result, the down-regulated ANGPT1 by increased miR-466 and miR-200 activities contributes to decreased angiogenesis and ineffective wound tissue repair under the diabetic conditions.

does not play a dominant role in IRE1 α -regulated BMPC angiogenesis in diabetes. XBP1 knockdown did not induce significant impairment of BMPC function either (Fig. 2G–I). Importantly, our data show that neither miR expression nor upregulation of miRs caused by IRE1 α deletion can be affected by activation of XBP1, suggesting that XBP1 does not function congruously with IRE1 α on miR biogenesis. As a matter of fact, XBP1 has been reported to induce miR expression under certain circumstances (49,50), probably due to its role in the activation of gene expression as a transcription factor. Although the mechanism by which IRE1 α selectively processes RNA substrates (miRs or *XBP1* mRNA) remains to be elucidated, our study suggested that the IRE1 α -regulated BMPC functional change and miR biogenesis in diabetes are independent of XBP1, a scenario distinct from the canonical IRE1 α -UPR signaling pathway under the pharmacological or acute ER stress conditions.

Recent studies have uncovered a new dimension in which miRs regulate cellular behavior in response to physiological and pathophysiological stress (51). In this study, through miR microarray, we identified 44 significantly

altered miRs in diabetic BMPCs, 31 of which were elevated (Fig. 3A). Previously, we found out that expression of Dicer, the rate-limiting enzyme that produces functional miRs, was decreased in diabetic BMPCs (17). On the basis of this, it was predicted that the majority of miRs in diabetic BMPCs are supposed to decrease. However, in this study, we have identified a subset of stress miRs that are controlled by IRE1 α RNase activity and are actively participating in regulating BMPC function. IRE1 α deletion results in a group of significantly upregulated miRs, many of which were similarly elevated in diabetic BMPCs (Fig. 3B and E). On the other hand, overexpression of IRE1 α suppresses the expression of these miRs (Fig. 4A). This unveils the possibility that IRE1 α may interfere with miR biogenesis and that impaired IRE1 α RNase activity leads to the elevation of mature miRs in diabetes. Furthermore, pre-miR-466 and pre-miR-200 in IRE1 α ^{-/-} BMPCs yielded significantly higher levels of mature miR-466 and miR-200s than that in the control BMPCs, indicating that IRE1 α -induced reduction of miR biogenesis happened at the pre-miR level. Pre-miR-466 and pre-miR-200 are processed by IRE1 α RNase because these two precursor miRs possess G/C sites at the stem-loop structure that match the IRE1 α RNase target motif (Fig. 3F) (29). The IRE1 α -mediated miR cleave assay indicated that pre-miR-466 and pre-miR-200 were indeed the RNA substrates of IRE1 α RNase activity (Fig. 3I). Importantly, augmentation of diabetic BMPC angiogenic function by restoring IRE1 α activities was compromised by overexpression of pre-miR-466 and pre-miR-200 (Fig. 5A and B), indicating that the downregulation of miR-466 and miR-200 by IRE1 α is critical to maintain effective angiogenesis in diabetes. In addition, we overexpressed Dicer in *db/db* BMPCs using adenovirus-mediated gene transfer and observed BMPC tube formation (Supplementary Fig. 2A). Our results indicated that overexpression of Dicer improved BMPC tube formation (Supplementary Fig. 2B and C), compared with their diabetic control. The previous report and ours indicated that Dicer controls a subset of miRs that improve angiogenesis (proangiogenic miRs) (17,52,53). Therefore, even though both Dicer and IRE1 α improve angiogenesis and regulate miR biogenesis, Dicer and IRE1 α improve angiogenesis and regulate miR biogenesis through distinct mechanisms.

Our study also provides the first evidence that miR-466 and miR-200 function in the same direction to regulate angiogenesis by targeting the same gene under the diabetic condition. Although previous reports have found that each of the miR-466 and miR-200 family miRs targets different genes in diverse types of cells (54–56), our study has confirmed that ANGPT1 is the direct target of miR-466 and miR-200 family miRs in BMPCs, as indicated by mRNA 3'-UTR binding assay and the gene and protein expression analysis (Fig. 6A–D). As a matter of fact, these two miR families have been reported to similarly respond to detrimental cellular stress and share common target genes, for

example, *Nfat5* in immune cells and *Dcx* and *Patah1b1* in neural stem cells (57,58). Our study delineated an important regulatory mechanism of miR-466 and miR-200 against the diabetic environment, in which the UPR transducer IRE1 α functions as the upstream regulator and the proangiogenic factor ANGPT1 acts as an effector. Therefore, IRE1 α -mediated miR decay represents a noncanonical UPR signaling that exerts an important role in promoting BMPC angiogenesis by protecting ANGPT1 from the miR attack under the diabetic condition.

The importance of IRE1 α in angiogenesis has been further investigated in diabetic wound healing through the cell- or direct gene transfer-based therapeutic approach. IRE1 α -expressing diabetic BMPCs demonstrated equal efficacy in promoting wound healing as normal BMPCs did, suggesting the effect of *IRE1 α* gene transfer on restoring diabetic BMPC function, which was consistent with our *in vitro* findings. One of the important mechanisms contributing to the acceleration of diabetic wound healing by IRE1 α expression was through promoting angiogenesis, as demonstrated by increased capillary density in wound beds (Fig. 7D). Additionally, wounds that received IRE1 α -expressing BMPCs were covered by a slightly keratinized epidermis layer upon wound closure (Fig. 7C and D), suggesting that IRE1 α -expressing BMPC therapy may facilitate wound re-epithelialization. This newly formed epidermis layer may be due to accelerated keratinocyte migration from the wound edge or may be constituted by the transformation of transplanted BMPCs, an interesting question to be elucidated in the future. The direct gene transfer of IRE1 α to the diabetic wounds, however, did not prove as effective as the cell therapies. This may be due to the disrupted cellular components within the diabetic wound bed, which comprised the overall improvement of healing in the direct gene transfer approach. Additionally, we should clarify that there are paradoxical changes in angiogenesis coexisting in different tissues in diabetes. Diabetes possesses the phenotype of excessive formation of premature blood vessels in retina and a defect in the formation of small blood vessels in peripheral tissues, such as the skin. Our findings could be specific for peripheral angiogenesis but not diabetic retinopathy. In summary, our studies provide a novel concept that the IRE1 α -mediated noncanonical UPR pathway plays an important role in promoting angiogenesis in diabetes. The related findings have important implications in tissue repair and regeneration associated with diabetic wounds.

Acknowledgments. The authors thank the staff from the Department of Laboratory Animal Research at Wayne State University for providing excellent care for the animals.

Funding. This work is supported by National Institutes of Health/National Institute of Diabetes and Digestive and Kidney Diseases grants R01 DK109036-01 (to J.-M.W.), R01 DK090313-05, and ES017829 and the American Heart Association grants 09GRNT2280479 (to K.Z.) and 13SDG16930098.

Duality of Interest. No potential conflicts of interest relevant to this article were reported.

Author Contributions. J.-M.W. designed research studies, conducted experiments for *in vivo* wound healing experiments, analyzed data from *in vitro* and *in vivo* experiments, and wrote the manuscript. Y.Q. assisted with experiments for BMPC culture and data acquisition. Z.-q.Y. and L.L. contributed to data interpretation. K.Z. contributed to the experimental design, data analysis, and interpretation; edited the manuscript; and provided the key reagents. J.-M.W. and K.Z. are the guarantors of this work and, as such, had full access to all the data in the study and take responsibility for the integrity of the data and the accuracy of the data analysis.

References

- Centers for Disease Control and Prevention. 2014 National Diabetes Statistics Report. Available from <http://www.cdc.gov/diabetes/data/statistics/2014StatisticsReport.html>. Accessed 24 October 2014
- Demidova-Rice TN, Durham JT, Herman IM. Wound healing angiogenesis: innovations and challenges in acute and chronic wound healing. *Adv Wound Care (New Rochelle)* 2012;1:17–22
- Asahara T, Murohara T, Sullivan A, et al. Isolation of putative progenitor endothelial cells for angiogenesis. *Science* 1997;275:964–967
- Tepper OM, Galiano RD, Capla JM, et al. Human endothelial progenitor cells from type II diabetics exhibit impaired proliferation, adhesion, and incorporation into vascular structures. *Circulation* 2002;106:2781–2786
- Loomans CJ, de Koning EJ, Staal FJ, et al. Endothelial progenitor cell dysfunction: a novel concept in the pathogenesis of vascular complications of type 1 diabetes. *Diabetes* 2004;53:195–199
- Yalcin A, Hotamisligil GS. Impact of ER protein homeostasis on metabolism. *Diabetes* 2013;62:691–693
- Zhang K, Kaufman RJ. From endoplasmic-reticulum stress to the inflammatory response. *Nature* 2008;454:455–462
- Zhang K, Kaufman RJ. The unfolded protein response: a stress signaling pathway critical for health and disease. *Neurology* 2006;66(Suppl. 1):S102–S109
- Hollien J, Weissman JS. Decay of endoplasmic reticulum-localized mRNAs during the unfolded protein response. *Science* 2006;313:104–107
- Upton JP, Wang L, Han D, et al. IRE1 α cleaves select microRNAs during ER stress to derepress translation of proapoptotic Caspase-2. *Science* 2012;338:818–822
- So JS, Hur KY, Tarrío M, et al. Silencing of lipid metabolism genes through IRE1 α -mediated mRNA decay lowers plasma lipids in mice. *Cell Metab* 2012;16:487–499
- Tam AB, Koong AC, Niwa M. Ire1 has distinct catalytic mechanisms for XBP1/HAC1 splicing and RIDD. *Cell Reports* 2014;9:850–858
- Lin JH, Li H, Yasumura D, et al. IRE1 signaling affects cell fate during the unfolded protein response. *Science* 2007;318:944–949
- Kim I, Xu W, Reed JC. Cell death and endoplasmic reticulum stress: disease relevance and therapeutic opportunities. *Nat Rev Drug Discov* 2008;7:1013–1030
- Bartel DP. MicroRNAs: genomics, biogenesis, mechanism, and function. *Cell* 2004;116:281–297
- Bae ON, Wang JM, Baek SH, Wang Q, Yuan H, Chen AF. Oxidative stress-mediated thrombospondin-2 upregulation impairs bone marrow-derived angiogenic cell function in diabetes mellitus. *Arterioscler Thromb Vasc Biol* 2013;33:1920–1927
- Wang JM, Tao J, Chen DD, et al. MicroRNA miR-27b rescues bone marrow-derived angiogenic cell function and accelerates wound healing in type 2 diabetes mellitus. *Arterioscler Thromb Vasc Biol* 2014;34:99–109
- Maurel M, Chevet E. Endoplasmic reticulum stress signaling: the microRNA connection. *Am J Physiol Cell Physiol* 2013;304:C1117–C1126
- Christian P, Su Q. MicroRNA regulation of mitochondrial and ER stress signaling pathways: implications for lipoprotein metabolism in metabolic syndrome. *Am J Physiol Endocrinol Metab* 2014;307:E729–E737
- Zhang K, Wang S, Malhotra J, et al. The unfolded protein response transducer IRE1 α prevents ER stress-induced hepatic steatosis. *EMBO J* 2011;30:1357–1375
- Wang JM, Isenberg JS, Billiar TR, Chen AF. Thrombospondin-1/CD36 pathway contributes to bone marrow-derived angiogenic cell dysfunction in

- type 1 diabetes via Sonic hedgehog pathway suppression. *Am J Physiol Endocrinol Metab* 2013;305:E1464–E1472
22. Park SW, Zhou Y, Lee J, et al. The regulatory subunits of PI3K, p85 α and p85 β , interact with XBP-1 and increase its nuclear translocation. *Nat Med* 2010;16:429–437
23. Yang L, Xue Z, He Y, Sun S, Chen H, Qi L. A Phos-tag-based approach reveals the extent of physiological endoplasmic reticulum stress. *PLoS One* 2010; 5:e11621
24. Felli N, Fontana L, Pelosi E, et al. MicroRNAs 221 and 222 inhibit normal erythropoiesis and erythroleukemic cell growth via kit receptor down-modulation. *Proc Natl Acad Sci USA* 2005;102:18081–18086
25. Balaji S, LeSaint M, Bhattacharya SS, et al. Adenoviral-mediated gene transfer of insulin-like growth factor 1 enhances wound healing and induces angiogenesis. *J Surg Res* 2014;190:367–377
26. Schröder K, Kohlen A, Aicher A, et al. NADPH oxidase Nox2 is required for hypoxia-induced mobilization of endothelial progenitor cells. *Circ Res* 2009;105: 537–544
27. Dominici M, Le Blanc K, Mueller I, et al. Minimal criteria for defining multipotent mesenchymal stromal cells. The International Society for Cellular Therapy position statement. *Cytotherapy* 2006;8:315–317
28. Hulsmans M, De Keyser D, Holvoet P. MicroRNAs regulating oxidative stress and inflammation in relation to obesity and atherosclerosis. *FASEB J* 2011;25: 2515–2527
29. Prischi F, Nowak PR, Carrara M, Ali MM. Phosphoregulation of Ire1 RNase splicing activity. *Nat Commun* 2014;5:3554
30. Takakura N, Watanabe T, Suenobu S, et al. A role for hematopoietic stem cells in promoting angiogenesis. *Cell* 2000;102:199–209
31. Jeansson M, Gawlik A, Anderson G, et al. Angiopoietin-1 is essential in mouse vasculature during development and in response to injury. *J Clin Invest* 2011;121:2278–2289
32. Cho CH, Sung HK, Kim KT, et al. COMP-angiopoietin-1 promotes wound healing through enhanced angiogenesis, lymphangiogenesis, and blood flow in a diabetic mouse model. *Proc Natl Acad Sci U S A* 2006;103:4946–4951
33. Koh GY. Orchestral actions of angiopoietin-1 in vascular regeneration. *Trends Mol Med* 2013;19:31–39
34. Tao J, Yang Z, Wang JM, et al. Shear stress increases Cu/Zn SOD activity and mRNA expression in human endothelial progenitor cells. *J Hum Hypertens* 2007;21:353–358
35. Zhang M, Malik AB, Rehman J. Endothelial progenitor cells and vascular repair. *Curr Opin Hematol* 2014;21:224–228
36. Harding HP, Ron D. Endoplasmic reticulum stress and the development of diabetes: a review. *Diabetes* 2002;51(Suppl. 3):S455–S461
37. Back SH, Kaufman RJ. Endoplasmic reticulum stress and type 2 diabetes. *Annu Rev Biochem* 2012;81:767–793
38. Lee J, Ozcan U. Unfolded protein response signaling and metabolic diseases. *J Biol Chem* 2014;289:1203–1211
39. Cheng R, Ma JX. Angiogenesis in diabetes and obesity. *Rev Endocr Metab Disord* 2015;16:67–75
40. Zhang K, Kaufman RJ. Protein folding in the endoplasmic reticulum and the unfolded protein response. *Handb Exp Pharmacol* 2006;69–91
41. Fu S, Watkins SM, Hotamisligil GS. The role of endoplasmic reticulum in hepatic lipid homeostasis and stress signaling. *Cell Metab* 2012;15:623–634
42. Yang L, Calay ES, Fan J, et al. METABOLISM. S-nitrosylation links obesity-associated inflammation to endoplasmic reticulum dysfunction. *Science* 2015; 349:500–506
43. Hollien J, Lin JH, Li H, Stevens N, Walter P, Weissman JS. Regulated Ire1-dependent decay of messenger RNAs in mammalian cells. *J Cell Biol* 2009;186: 323–331
44. Han D, Lerner AG, Vande Walle L, et al. IRE1 α kinase activation modes control alternate endoribonuclease outputs to determine divergent cell fates. *Cell* 2009;138:562–575
45. Coelho DS, Gaspar CJ, Domingos PM. Ire1 mediated mRNA splicing in a C-terminus deletion mutant of *Drosophila* Xbp1. *PLoS One* 2014;9:e105588
46. Bhatta M, Ma JH, Wang JJ, Sakowski J, Zhang SX. Enhanced endoplasmic reticulum stress in bone marrow angiogenic progenitor cells in a mouse model of long-term experimental type 2 diabetes. *Diabetologia* 2015;58:2181–2190
47. Brown MK, Naidoo N. The endoplasmic reticulum stress response in aging and age-related diseases. *Front Physiol* 2012;3:263
48. Zeng L, Xiao Q, Chen M, et al. Vascular endothelial cell growth-activated XBP1 splicing in endothelial cells is crucial for angiogenesis. *Circulation* 2013;127:1712–1722
49. Bartoszewski R, Brewer JW, Rab A, et al. The unfolded protein response (UPR)-activated transcription factor X-box-binding protein 1 (XBP1) induces microRNA-346 expression that targets the human antigen peptide transporter 1 (TAP1) mRNA and governs immune regulatory genes. *J Biol Chem* 2011;286: 41862–41870
50. Zeng L, Li Y, Yang J, et al. XBP 1-deficiency abrogates neointimal lesion of injured vessels via cross talk with the PDGF signaling. *Arterioscler Thromb Vasc Biol* 2015;35:2134–2144
51. Mendell JT, Olson EN. MicroRNAs in stress signaling and human disease. *Cell* 2012;148:1172–1187
52. Kuehbacher A, Urbich C, Zeiher AM, Dimmeler S. Role of Dicer and Drosha for endothelial microRNA expression and angiogenesis. *Circ Res* 2007;101:59–68
53. Suárez Y, Fernández-Hernando C, Pober JS, Sessa WC. Dicer dependent microRNAs regulate gene expression and functions in human endothelial cells. *Circ Res* 2007;100:1164–1173
54. Seo M, Choi JS, Rho CR, Joo CK, Lee SK. MicroRNA miR-466 inhibits lymphangiogenesis by targeting prospero-related homeobox 1 in the alkali burn corneal injury model. *J Biomed Sci* 2015;22:3
55. Park SM, Gaur AB, Lengyel E, Peter ME. The miR-200 family determines the epithelial phenotype of cancer cells by targeting the E-cadherin repressors ZEB1 and ZEB2. *Genes Dev* 2008;22:894–907
56. Baseler WA, Thapa D, Jagannathan R, Dabkowski ER, Croston TL, Hollander JM. miR-141 as a regulator of the mitochondrial phosphate carrier (Slc25a3) in the type 1 diabetic heart. *Am J Physiol Cell Physiol* 2012;303:C1244–C1251
57. Luo Y, Liu Y, Liu M, et al. Sfrmbt2 10th intron-hosted miR-466(a/e)-3p are important epigenetic regulators of Nfat5 signaling, osmoregulation and urine concentration in mice. *Biochim Biophys Acta* 2014;1839:97–106
58. Shyamasundar S, Jadhav SP, Bay BH, et al. Analysis of epigenetic factors in mouse embryonic neural stem cells exposed to hyperglycemia. *PLoS One* 2013; 8:e65945